JOURNAL OF DIFFERENCE EQUATIONS AND APPLICATIONS, 2016
VOL. 22, NO. 7, 913–940
http://dx.doi.org/10.1080/10236198.2016.1162161

Taylor & Francis
Taylor & Francis Group

# Travelling wave solutions of multisymplectic discretizations of semi-linear wave equations

Fleur McDonald[a], Robert I. McLachlan[a], Brian E. Moore[b] and G. R. W. Quispel[c]

[a]Institute of Fundamental Sciences, Massey University, Palmerston North, New Zealand; [b]Department of Mathematics, University of Central Florida, Orlando, FL, USA; [c]Department of Mathematics and Statistics, La Trobe University, Melbourne, Australia

**ABSTRACT**

How well do multisymplectic discretisations preserve travelling wave solutions? To answer this question, the 5-point central difference scheme is applied to the semi-linear wave equation. A travelling wave ansatz leads to an ordinary difference equation whose solutions can be compared to travelling wave solutions of the PDE. For a discontinuous nonlinearity the difference equation is solved exactly. For continuous nonlinearities the difference equation is solved using a Fourier series, and resonances that depend on the grid-size are revealed for a smooth nonlinearity. In general, the infinite dimensional functional equation, which must be solved to get the travelling wave solutions, is intractable, but backward error analysis proves to be a powerful tool, as it provides a way to study the solutions of equation through a simple ODE that describes the behavior to arbitrarily high order. A general framework for using backward error analysis to analyze preservation of travelling waves for other equations and discretisations is presented. Then, the advantages that multisymplectic methods have over other methods are briefly highlighted.

**ARTICLE HISTORY**
Received 22 October 2015
Accepted 29 February 2015

**KEYWORDS**
Five-point centered difference; backward error analysis; travelling wave solution; semi-linear wave equation; resonance

**AMS SUBJECT CLASSIFICATIONS**
65M22; 65P10; 35C07; 35L05

## 1. Introduction

Since their introduction by Marsden et al. [20] and Reich [29], multisymplectic integrators have seen a huge growth in interest, because they offer the prospect of getting the same excellent long-time results for Hamiltonian PDEs that symplectic integrators do for ODEs [7,18,24]. The Hamiltonian ODE $Kz_t = \nabla S(z)$, where $z \in \mathbb{R}^d$, $K$ is an invertible $d \times d$ antisymmetric matrix and $S\colon \mathbb{R}^d \to \mathbb{R}$ is the Hamiltonian, obeys conservation of symplecticity: $\omega_t = 0$, where $\omega = \mathrm{d}z \wedge K\mathrm{d}z$. The maps $z_n \to z_{n+1}$ obtained from symplectic integrators obey $\omega_{n+1} = \omega_n$. In contrast, the multiHamiltonian PDE

$$Kz_t + Lz_x = \nabla S(z) \tag{1}$$

where $K$ and $L$ are antisymmetric $d \times d$ matrices, obeys the multisymplectic conservation law $\omega_t + \kappa_x = 0$, where $\omega = \mathrm{d}z \wedge K\mathrm{d}z$ and $\kappa = \mathrm{d}z \wedge L\mathrm{d}z$. Multisymplectic integrators have a fully discrete conservation law which is a discretization of the continuous one.

**CONTACT** Robert I. McLachlan R.McLachlan@massey.ac.nz

There are a number of apparent advantages to multisymplectic integrators. They are in some sense the simplest natural discrete analogue of (1). Many standard methods that have been in use for a long time are multisymplectic, such as the 5-point stencil for the wave equation. They obey a discrete variational principle. Because the conservation law is local, they allow a flexible treatment of boundary conditions. They are nondissipative. They appear to work well in many numerical experiments on integrable and nonintegrable PDEs.

However, some differences between the PDE and ODE case are immediately apparent. (i) In the PDE case, the matrices $K$ and $L$ can be singular, and so the 2-forms $\omega$ and $\kappa$ can be degenerate. (ii) In the ODE case, the discretization of the conservation law is unique, and is identical to the one obeyed by the flow of the ODE, whereas in the PDE case, the discretization of the conservation law is not unique and is necessarily an approximation of that obeyed by the PDE. (iii) In the ODE, preservation of the symplectic form is known to be fundamental to the dynamics of Hamiltonian systems, and is used either implicitly or explicitly in all studies of Hamiltonian dynamics. In the PDE, use of a multisymplectic conservation law is hardly known. It is not clear if this is because the study of the dynamics of PDEs itself is relatively less developed, or because the conservation law itself is relatively weak. The results and observations available for multisymplectic integrators so far are not as strong as those available for symplectic integrators, which include backward error analysis, long-time energy behaviour, and preservation of invariant sets such as periodic and quasiperiodic orbits.

Nevertheless, multisymplectic schemes have been shown to preserve more than just the multisymplectic conservation law. For example, the Gauss–Legendre Runge–Kutta methods satisfy fully discrete energy and momentum conservation laws for linear equations [6,29]. The Preissmann box scheme and the Euler box scheme satisfy semi-discrete energy and momentum conservation laws for nonlinear equations [27,28]. Other properties preserved by certain multisymplectic methods include phase space structure [17], conservation of wave action [13], dispersion relations and group velocity [1,14], and other conservation laws that result from Noether's theorem [10,28].

In this paper, we study the preservation of travelling waves under multisymplectic discretization. Many PDEs, such as the Boussinesq, Schrödinger, Korteweg–de Vries, and nonlinear wave equations (among others), have travelling wave solutions, and the multi-Hamiltonian forms for these conservative PDEs are known (cf. [2–5]). (Note that some equations can be written in the multi-Hamiltonian form (1) in multiple ways [19].)

Our focus is on the semi-linear wave equation

$$u_{tt} = u_{xx} - V'(u). \tag{2}$$

Travelling waves are solutions to the PDE that travel at a constant speed $c$ without changing shape. Thus, they take the form $u(x,t) = \varphi(x-ct)$. The PDE (2) has a 2-parameter group of symmetries given by translations in $x$ and $t$; thus travelling waves are relative equilibria with respect to a subgroup of this symmetry group. Introducing the travelling wave coordinate $\xi := x - ct$, the PDE (2) is reduced to the ODE

$$(c^2 - 1)\varphi_{\xi\xi}(\xi) = -V'(\varphi(\xi)). \tag{3}$$

This is a planar Hamiltonian system. Introducing the conjugate momentum $\psi := (c^2 - 1)\varphi_\xi$, with $(c^2 - 1)$ playing the role of mass, its Hamiltonian form is

$$\varphi_\xi = \frac{\partial H}{\partial \psi}, \qquad \psi_\xi = -\frac{\partial H}{\partial \varphi} \qquad \text{with} \qquad H = \frac{1}{2}(c^2 - 1)^{-1}\psi^2 + V(\varphi). \tag{4}$$

Its phase portrait is easily determined from the level sets of the reduced Hamiltonian $H$. Bounded solutions are either solitary waves (that obey $\varphi'(\pm\infty) = 0$) or periodic travelling waves. Solitary waves (sometimes called pulses, wave fronts, kinks, or anti-kinks) correspond to homoclinic ($\varphi(\infty) = \varphi(-\infty)$) or heteroclinic ($\varphi(\infty) \neq \varphi(-\infty)$) orbits of (3), and require an infinite spatial domain. Periodic travelling waves correspond to periodic solutions of (3) and may exist on a periodic or infinite spatial domain.

Multisymplectic integrators for equation (2) have been constructed using discrete variational principles [20], and by applying symplectic Runge–Kutta [25,29,30] and partitioned Runge–Kutta [16,26,30,31] methods in space and time. In this paper we consider one particular multisymplectic integrator, the 5-point central difference method for (2) given by

$$\frac{1}{(\Delta t)^2}\left(u_i^{n+1} - 2u_i^n + u_i^{n-1}\right) - \frac{1}{(\Delta x)^2}\left(u_{i+1}^n - 2u_i^n + u_{i-1}^n\right) = -V'(u_i^n). \tag{5}$$

This can be viewed either as the 2-stage Lobatto IIIA–IIIB partitioned Runge–Kutta method applied in space and time with a particular choice of partitioning [31], as the Euler–Lagrange equations of the discrete Lagrangian [27], or simply as the leapfrog method in space and time.

We seek general travelling wave solutions of the discrete equation (5) of the form

$$u_i^n = \varphi(x_i - ct_n) = \varphi(i\Delta x - cn\Delta t) = \varphi(i\sigma - n\kappa) = \varphi(\xi) \tag{6}$$

where $\sigma = \Delta x$, $\kappa = c\Delta t$, and $\xi = i\sigma - n\kappa$. The two parameters $\sigma$ and $\kappa$ will play an important role in the description of discrete travelling waves. The substitution $u_i^n = \varphi(\xi)$ into the scheme (5) yields the *discrete travelling wave equation*

$$\begin{aligned} &\frac{c^2}{\kappa^2}\left(\varphi(\xi + \kappa) - 2\varphi(\xi) + \varphi(\xi - \kappa)\right) \\ &\qquad - \frac{1}{\sigma^2}\left(\varphi(\xi + \sigma) - 2\varphi(\xi) + \varphi(\xi - \sigma)\right) = -V'(\varphi(\xi)). \end{aligned} \tag{7}$$

Ideally, one would like to understand all solutions of (7) under broad conditions on $c$, $\kappa$, $\sigma$, $V$, and $\varphi$ – for example, $V$ smooth and $\varphi$ bounded for all $\xi \in \mathbb{R}$. This entire family of discrete travelling waves could then be compared to the continuous family. It is immediately apparent that the parameter $\sigma/\kappa$ is of crucial importance. When $\sigma/\kappa = m_1/m_2$ is rational, (7) is a finite-dimensional map. It then makes the most sense to look for solutions with $\xi \in \frac{\sigma}{m_1}\mathbb{Z}$. When $\sigma/\kappa$ is irrational, we need to take $\xi \in \mathbb{R}$ and seek solutions in some space of functions to be determined from (7) itself. In this case, (7) is an infinite-dimensional functional equation. Thus, at first sight, the drastic reduction in complexity that is obtained in the continuous case (from a PDE to a planar ODE) is not obtained in the discrete case.

We approach Equation (7) from two distinct points of view; hence, the article is divided into two parts. In Part I, *case studies* are used to construct solutions of (7) and carefully compare them to the solutions of (3) for three special cases of the nonlinearity:

(1) a discontinuous $V'$ given by the McKean caricature of the cubic, in Section 2.1,
(2) a continuous but non-smooth $V'$ given by the sawtooth nonlinearity, in Section 2.2,
(3) a smooth $V'$ given by the sine nonlinearity, in Section 2.3.

Our main contributions in Part I are:

- Comparison of discrete and continuous travelling waves providing details of the extent to which travelling waves are preserved by the discretisation.
- Exposition of tools and techniques for constructing and analyzing solutions of (7).
- Exploration of resonances that depend on $\kappa$ and $\sigma$ for a smooth nonlinearity.

In Part II, *backward error analysis* is used to give a highly accurate description of the discrete travelling waves, as well as the way in which they approximate the continuous travelling waves. This more general approach allows for considerations of a wider range of problems, which is illustrated in two sections.

(1) Application of backward error analysis for (7) with arbitrary $V'$, in Section 3.1.
(2) Demonstration of how backward error analysis may be used to study travelling waves for other multisymplectic discretizations and multi-Hamiltonian equations, in Section 3.2.

Our main contributions in Part II are:

- Introduction of an original and extremely powerful application of backward error analysis to the study of discrete travelling waves, which reduces (in the sense of backward error) an intractable infinite-dimensional functional equation to a simple ODE.
- Confirmation that the travelling wave solutions of the modified equations (obtained through backward error analysis) represent the numerical solution, which results from a multisymplectic discretisation, and mimic the travelling waves of the PDE.
- Development of a framework for analyzing the travelling wave solutions of the modified equations obtained through backward error analysis for other multi-symplectic discretisations of more general multi-Hamiltonian PDEs.

Finally, a juxtaposition of multisymplectic and non-symplectic (especially symmetric) methods for the steady-state solutions (in the Appendix 1) provides a useful and interesting contrast of the numerical solution behavior, revealing a special advantage of multisymplectic methods.

## 2. Part I. case studies

Travelling wave solutions of the multi-symplectic discretization (5) are obtained by solving the ordinary difference Equation (7) for some specific cases of $V'$. Similar studies have been performed in different contexts. Most relevant are the results of Cahn et al. [8], which construct exact travelling wave solutions for a spatially discrete Allen–Cahn equation, and, since equation they considered has two spatial dimensions, the steady-state equation is actually a special case of (7). In addition, equation solved in [8] has a McKean nonlinearity,

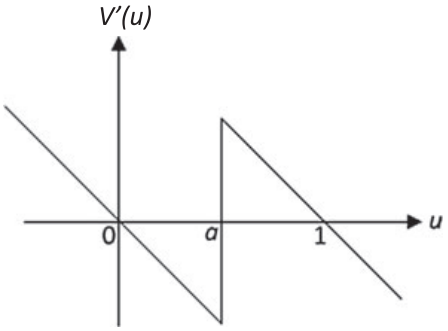


**Figure 1.** McKean nonlinearity: $-V'(u) = -u + \mathcal{H}(u-a)$.

which is used in our first case study, and our method of solution in that case follows the approach of [8].

### 2.1. Discontinuous $V'$: McKean nonlinearity

In a 1970 study of nerve conduction, McKean [22] proposed a caricature of the cubic function $x(x-a)(x-1)$. The McKean caricature (Figure 1) is given by

$$V'(u) = u - \mathcal{H}(u-a) \tag{8}$$

where $0 < a < 1$ and $\mathcal{H}$ is the Heaviside step function.

The function is discontinuous, but it has long been used in the study of travelling waves, and it provides a straightforward path to exact solutions of (3) and (7).

#### 2.1.1. Continuous travelling waves

Upon substituting (8) into (3), the travelling wave equation becomes

$$(c^2-1)\varphi''(\xi) = -\varphi(\xi) + \mathcal{H}(\varphi(\xi) - a), \tag{9}$$

where we require $|c| < 1$. The phase portrait of this ODE is shown in Figure 2. Notice that (9) possesses both periodic and heteroclinic travelling waves. For heteroclinic travelling waves we impose the boundary conditions

$$\lim_{\xi\to-\infty} \varphi(\xi) = 0, \qquad \lim_{\xi\to\infty} \varphi(\xi) = 1. \tag{10}$$

We expect a monotonic front solution, and, since $a \in (0,1)$, there must be $\xi^* \in \mathbb{R}$ for which

$$\varphi(\xi^*) = a \quad \text{with} \quad \varphi(\xi) < a \quad \text{for} \quad \xi < \xi^* \quad \text{and} \quad \varphi(\xi) > a \quad \text{for} \quad \xi > \xi^*. \tag{11}$$

Following [8], the continuous nonlinear problem (9) may be stated,

$$(c^2-1)\varphi''(\xi) = -\varphi(\xi) + \mathcal{H}(\xi - \xi^*), \tag{12}$$

which is linear. This is the essential reason for considering the McKean nonlinearity.

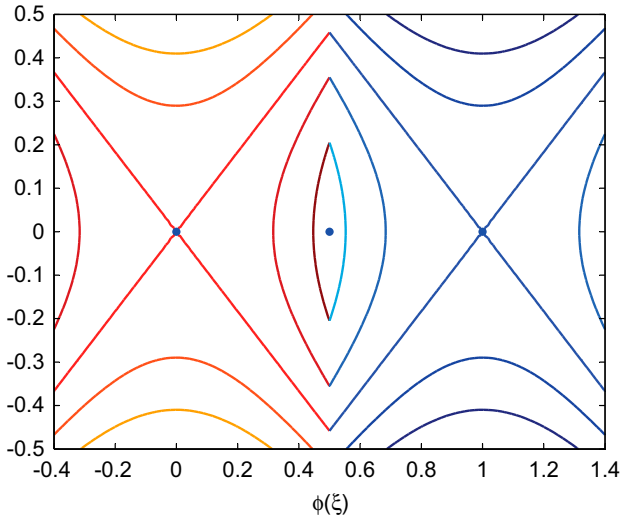


**Figure 2.** Phase portrait of (3) with the McKean nonlinearity.

We seek solutions of Equation (12) for which there exists an $\epsilon > 0$ such that $|\varphi(\xi)| \leq Ke^{\epsilon\xi}$ for $\xi < 0$ (see Lemma 4.1 of [8]). We apply the change of variables

$$\varphi_\epsilon(\xi) = e^{-\epsilon\xi}\varphi(\xi) \tag{13}$$

where $\epsilon > 0$ is sufficiently small, and obtain

$$(c^2-1)(2\epsilon\varphi_\epsilon'(\xi) + \varphi_\epsilon''(\xi)) + \varphi_\epsilon(\xi)(1+\epsilon^2(c^2-1)) = e^{-\epsilon\xi}\mathcal{H}(\xi-\xi^*).$$

Applying the Fourier transform,

$$\hat{\varphi}_\epsilon(s) = \int_{-\infty}^{\infty} e^{-is\xi}\varphi_\epsilon(\xi)\mathrm{d}\xi \tag{14}$$

and using the properties of Fourier transforms, we get

$$\hat{\varphi}_\epsilon(s) = \frac{e^{-(is+\epsilon)\xi^*}}{(is+\epsilon)R_{\mathrm{Cont}}(s-i\epsilon)}$$

where $R_{\mathrm{Cont}}(s) = 1 - c^2s^2 + s^2$. Next, we take the inverse Fourier transform,

$$\varphi_\epsilon(\xi) = \frac{1}{2\pi}\int_{-\infty}^{\infty} e^{is\xi}\hat{\varphi}_\epsilon(s)\mathrm{d}s, \tag{15}$$

giving the solution in the original variables as

$$\varphi(\xi) = \frac{1}{2\pi}\int_{-\infty}^{\infty} \frac{e^{(is+\epsilon)\xi}e^{-(is+\epsilon)\xi^*}}{(is+\epsilon)R_{\mathrm{Cont}}(s-i\epsilon)}\mathrm{d}s.$$

Taking the limit as $\epsilon \to 0$ and changing the limits of integration we get

$$\varphi(\xi) = \frac{1}{2\pi i}\int_{-i\epsilon-\infty}^{-i\epsilon+\infty} \frac{e^{is(\xi-\xi^*)}}{sR_{\mathrm{Cont}}(s)}\mathrm{d}s. \tag{16}$$

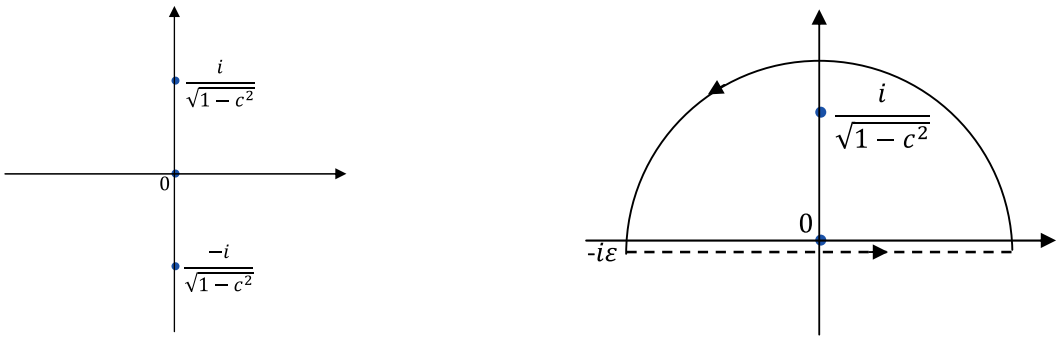


**Figure 3.** Singularities in the integrand of (16) and the contour used.

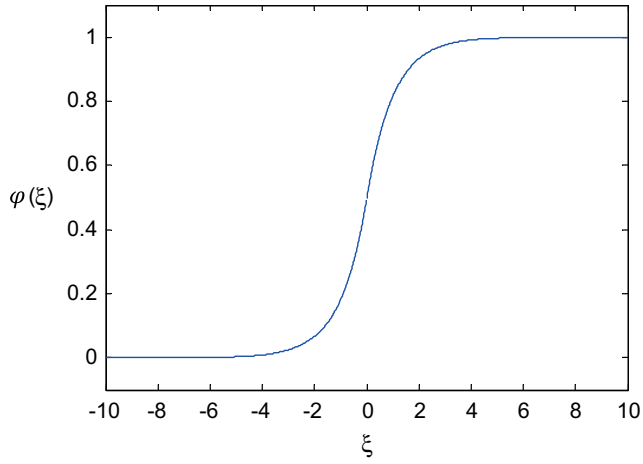


**Figure 4.** Travelling wave solution (17) of (3) with $c = 0.1$ and $\xi^* = 0$.

The domain of integration is changed slightly in order that residue theory can be applied to evaluate the improper integral. We can factorise $R_{\text{Cont}}(s)$ to get

$$R_{\text{Cont}}(s) = \left(1 - c^2\right)\left(s - \frac{i}{\sqrt{1-c^2}}\right)\left(s + \frac{i}{\sqrt{1-c^2}}\right).$$

Now, we evaluate the integral, noting singularities

$$s_0 = 0, \qquad s_1 = \frac{i}{\sqrt{1-c^2}}, \qquad s_2 = -\frac{i}{\sqrt{1-c^2}},$$

which are plotted in Figure 3 for $0 \leq c < 1$.

For $\xi > \xi^*$ we close the top half plane with a semi-circular region taking the real axis to $-i\epsilon$ (See Figure 3). The singularities enclosed by this region are $s_0$ and $s_1$. For $\xi < \xi^*$ we close the bottom half plane enclosing $s_2$. Hence, the explicit analytic solution for the continuous case is

$$\varphi(\xi) = \begin{cases} 1 - \frac{1}{2}e^{\frac{-(\xi-\xi^*)}{\sqrt{1-c^2}}} & \text{if } \xi > \xi^* \\ \frac{1}{2}e^{\frac{(\xi-\xi^*)}{\sqrt{1-c^2}}} & \text{if } \xi < \xi^* \end{cases} \tag{17}$$

which is a heteroclinic travelling wave, shown in Figure 4 for $c = 0.1$ and $\xi^* = 0$.

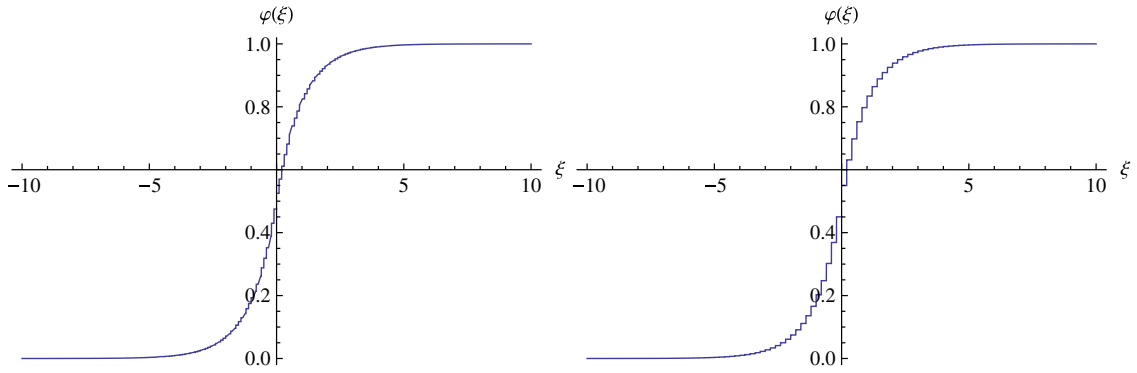


**Figure 5.** The solution of (7) for $c = 0$: $\kappa = 0.1$ left, $\kappa = 0.2$ right.

### 2.1.2. Discrete travelling waves

Now consider the discrete travelling wave Equation (7) with McKean nonlinearity. Using the same procedure as for the continuous case gives the solution

$$\varphi(\xi) = \frac{1}{2\pi i}\int_{-\infty}^{\infty} \frac{e^{is(\xi-\xi^*)}}{sR_{\text{Disc}}(s)}\mathrm{d}s \tag{18}$$

where

$$R_{\text{Disc}}(s) = 1 - \frac{2c^2}{\kappa^2}\left(1-\cos(\kappa s)\right) + \frac{2}{\sigma^2}\left(1-\cos(\sigma s)\right). \tag{19}$$

Finding the explicit solution $\varphi(\xi)$ for this discrete case all comes down to analyzing the function $R_{\text{Disc}}(s)$. For rational values of $\frac{\sigma}{\kappa}$, finding the zeros of $R_{\text{Disc}}(s)$ reduces to finding the roots of polynomials. We illustrate this in two cases.

**Case** $\sigma = \kappa$ Setting $\sigma = \kappa$ in (19) we get

$$R_{\text{Disc}}(s) = 1 + \frac{2}{\kappa^2}\left(1-\cos(\kappa s)\right)\left(1-c^2\right).$$

Setting $R_{\text{Disc}}(s) = 0$ for the above equation we get two zeros lying on the imaginary axis. The periodic images of these zeros are also zeros of $R_{\text{Disc}}(s)$ for $\sigma = \kappa$. The complete set of zeros of $R_{\text{Disc}}(s)$ for $\sigma = \kappa$ is given by,

$$s = \frac{\pm\arccos\left(1+\frac{\kappa^2}{2(1-c^2)}\right) \pm 2n\pi}{\kappa}$$

where $n = 1, 2, 3, \ldots$. There is also a zero at $s = 0$ from the denominator of the solution (18). The residues can be calculated and summed analytically, giving an explicit solution of the discrete travelling wave equation. Examples for $c = 0$ and for $c \neq 0$ are shown in Figures 5 and 6, respectively. In all cases the solution is monotonic and piecewise constant, and the tail at each end of the solution does not contain any wiggles.

**Case** $\sigma = 2\kappa$ We now get

$$R_{\text{Disc}}(s) = 1 - \frac{2c^2}{\kappa^2}\left(1-\cos(\kappa s)\right) + \frac{1}{2\kappa^2}\left(1-\cos(2\kappa s)\right).$$

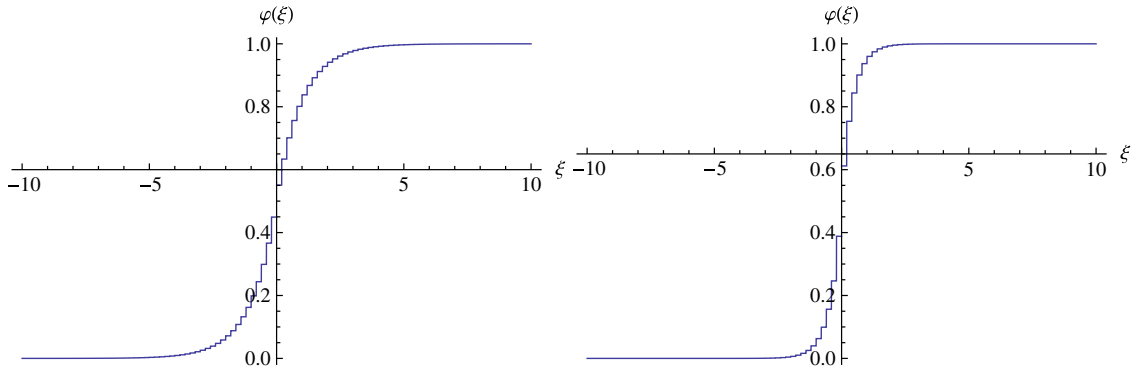


**Figure 6.** The solution of (7) for $\sigma = \kappa$: $c = 0.2$ left, $c = 0.9$ right.

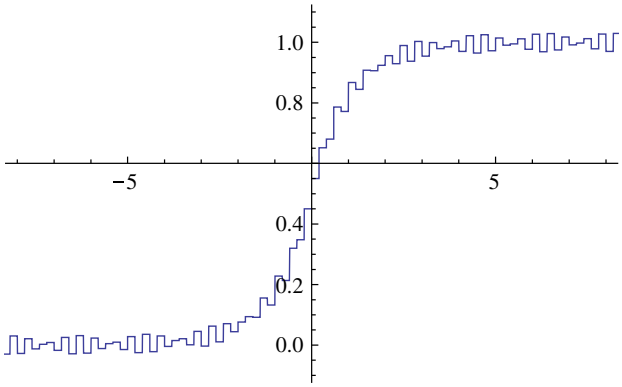


**Figure 7.** Solution of the discrete travelling wave equation with McKean nonlinearity for $\sigma = 2\kappa$.

The zeros of $R_{\mathrm{Disc}}(s)$ can be found explicitly. There are two complex roots and two real roots, plus their periodic images. The sum of the residues over the periodic images can be calculated explicitly in terms of hypergeometric functions. A typical solution is shown in Figure 7. Notice that we get a piecewise constant solution with wiggles at the tails. These wiggles, originating from the real zeros of $R_{\mathrm{Disc}}(s)$, have amplitude $\mathcal{O}(\kappa^2)$.

In theory, such an analytic solution can be found for any rational value of $\sigma/\kappa$, and in principle one could take a sequence of rational values approaching an irrational, although this would be very complicated. It is difficult to make conclusions about the existence of discrete travelling waves for irrational $\sigma/\kappa$ directly because this requires analyzing the convergence of the integral (18), which in turn requires detailed information about the zeros of the quasiperiodic function $R_{\mathrm{Disc}}(s)$.

### 2.1.3. Periodic travelling waves

Discrete periodic travelling waves of period $2\tau$, say, can be sought as Fourier series. First, set $\xi \in [0, 2\tau)$ so that

$$\mathcal{H}(\xi) = \begin{cases} 0 \text{ if } \xi \in [0, \tau) \\ 1 \text{ if } \xi \in (\tau, 2\tau). \end{cases}$$

Substituting the Fourier series

$$\varphi(\xi) = \sum_{n=-\infty}^{\infty} \tilde{\varphi}_n e^{in\frac{\pi}{\tau}\xi} \tag{20}$$

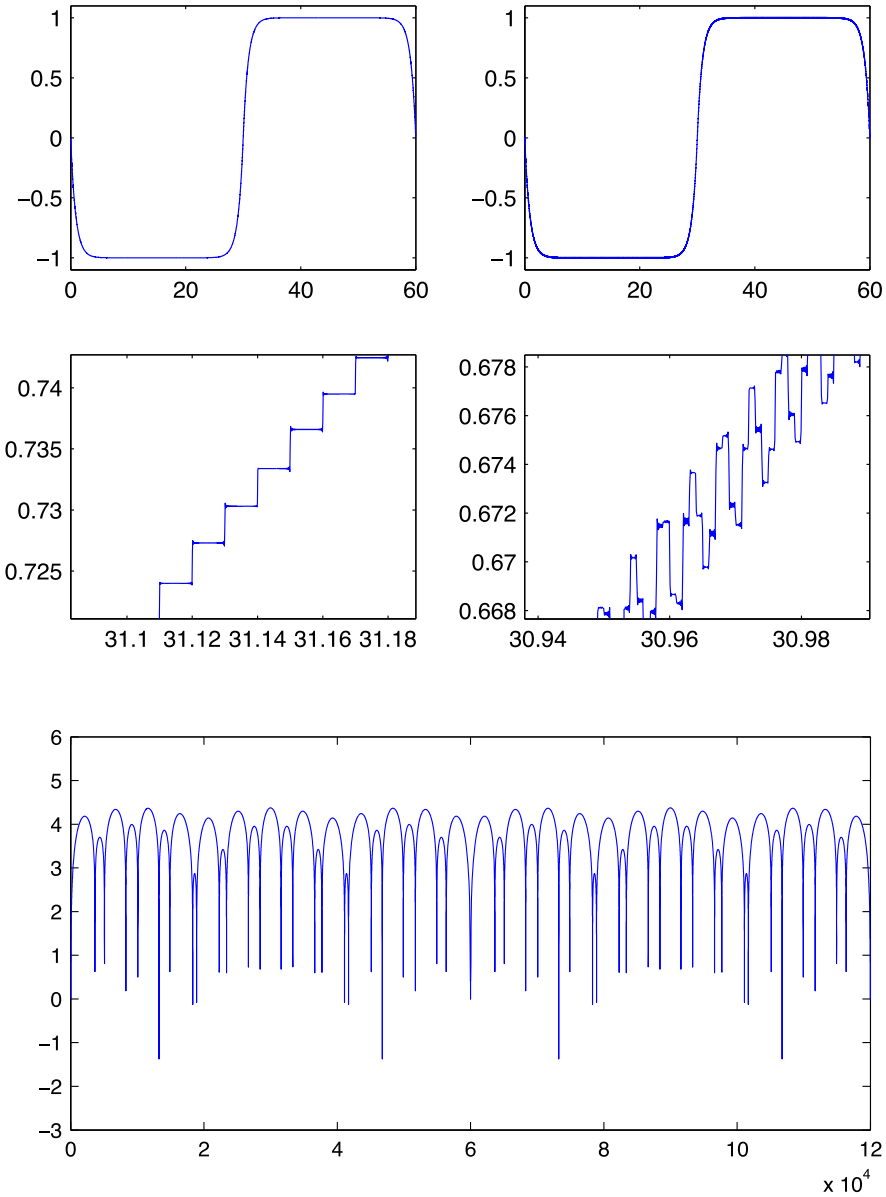


**Figure 8.** Periodic travelling waves of the leapfrog method with the McKean nonlinearity. When the space step $\sigma$, time step $\kappa$, and period $\tau$ are rationally related, travelling waves persist. Here we take $\tau = 30$ and $c = 1/2$ and approximate the waves with $2^{19}$ terms of a Fourier series. The left hand column shows the solution for $\sigma/\kappa = 2$, the right hand side for $\sigma/\kappa = 10/7$. The bottom figure shows the base-10 logarithm of the Fourier amplitudes for $r = 10/7$.

and

$$\mathcal{H}(\xi) = \sum_{n=-\infty}^{\infty} \tilde{h}_n e^{in\frac{\pi}{\tau}\xi}$$

into the difference equation (7) gives

$$\tilde{\varphi}_n = \frac{\tilde{h}_n}{1 + d_n}$$

where

$$d_n = \frac{2c^2}{\kappa^2}\left(\cos\left(\frac{n\pi\kappa}{\tau}\right) - 1\right) - \frac{2}{\sigma^2}\left(\cos\left(\frac{n\pi\sigma}{\tau}\right) - 1\right) \tag{21}$$

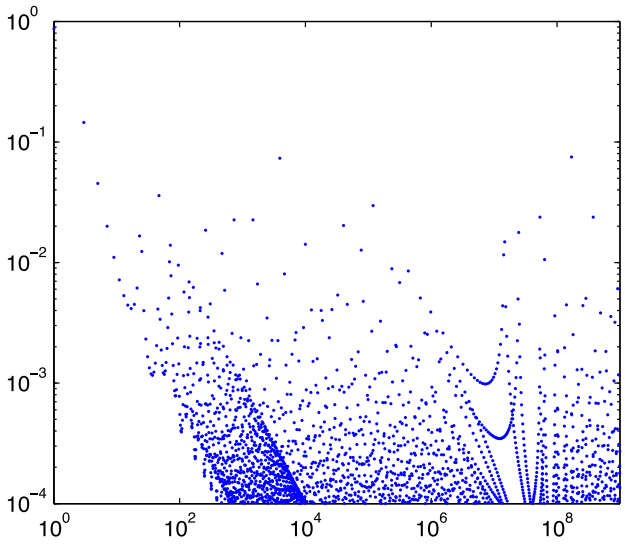


**Figure 9.** Fourier amplitudes of a putative discrete travelling wave using a McKean nonlinearity with $c = 1/2$, $\tau = 5\sqrt{2}$, $\sigma = 2/5$, and $\kappa = 1/5$. The Fourier amplitudes do not tend to zero, indicating nonconvergence of the Fourier series and nonexistence of a discrete travelling wave.

and

$$\tilde{h}_n = \frac{1}{in\pi}\left((-1)^n - 1\right).$$

If the Fourier series (20) converges, then it determines a discrete periodic travelling wave. We make observations on two cases.

**Case 1** If $\sigma$, $\kappa$, and $\tau$ are all rationally related (i.e. if $\sigma/\tau$, $\kappa/\tau \in \mathbb{Q}$), then the series (20) converges, assuming $d_n \neq 0$ for all odd $n$. In this case (20) is a finite sum of Fourier series of the form $\sum_{n=-\infty}^{\infty} e^{in\pi\xi/\tau}/(a+bn)$ $(a, b \in \mathbb{Z})$ which is the Fourier series of a piecewise-constant function. Some examples in which $\varphi(\xi)$ is approximated simply by truncating the sum are shown in Figure 8. The expected Gibbs phenomenon is seen, together with nonmonotonic behaviour of the solutions, similar to that seen in the heteroclinic case considered previously.

**Case 2** If either or both of $\sigma/\tau$ or $\kappa/\tau$ is irrational, then the sum (20) suffers from small denominators. A simple statistical model, in which $e^{in\pi\kappa/\tau}$ are uniformly distributed on the unit circle independently of $e^{in\pi\sigma/\tau}$, predicts that $(1-d_n)^{-1} = \mathcal{O}(n)$ and thus $\tilde{\varphi}_n = \mathcal{O}(1)$ and the series (20) does not converge. This prediction is borne out in examples. For example, Figure 9 shows $|\tilde{\varphi}_n|$ for $c = 1/2$, $\kappa = 1/5$, $\sigma = 2/5$, and $\tau = 5\sqrt{2}$. While for moderate $n$ the Fourier coefficients appear to be decreasing in magnitude, for $n \gtrsim 10^7$ the asymptotic behaviour $\tilde{\varphi}_n = \mathcal{O}(1)$ is clear.

We conclude that the McKean caricature *does* allow the explicit calculation of travelling waves for discretizations of Hamiltonian PDEs. The nonpreservation of travelling waves when $\sigma$, $\kappa$, and $\tau$ are not rationally related is not too suprising in view of the known sensitivity of periodic orbits of Hamiltonian ODEs to nonsmooth perturbations. Indeed, it appears that the McKean nonlinearity, despite being discontinuous at $u = a$, only just fails to be smooth enough – an extra factor of $\frac{1}{n}$ in $\tilde{h}_n$, which would arise if the forcing were merely continuous, would be enough to make the series (20) converge for all parameter values. This motivates our study in the next section of a continuous, piecewise linear nonlinearity.

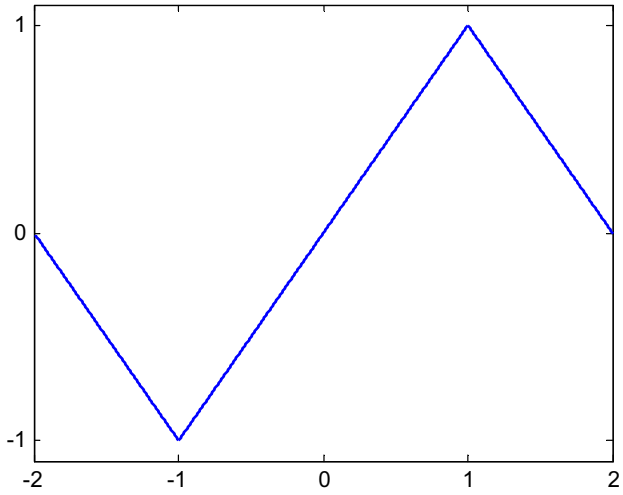


**Figure 10.** Sawtooth function $-V'(\varphi)$.

### 2.2. Continuous but non-smooth $V'$: Sawtooth nonlinearity

We now consider the continuous piecewise linear approximation of the cubic with domain $\varphi \in (-2, 2)$ given by

$$V'(\varphi) = \begin{cases} \varphi + 2, & -2 < \varphi < -1 \\ -\varphi, & -1 < \varphi < 1 \\ \varphi - 2, & 1 < \varphi < 2 \end{cases} \tag{22}$$

which is shown in Figure 10. The phase portrait of the ODE (3) with nonlinearity (22) is given in Figure 11, and shows that equation has heteroclinic and periodic travelling waves. We choose to concentrate on periodic travelling waves.

#### 2.2.1. Continuous travelling waves

Periodic solutions with amplitude greater than 1 will have the structure illustrated in Figure 11. We fix the period to be $2\tau$ and introduce the 6 marked points a,b,…,f. By translation symmetry, we are free to take $\varphi(0) = 0$ (point 'a'). We define $\xi^*$ as the least value of $\xi$ such that $\varphi(\xi^*) = 1$ (point 'b'). By symmetry, we then have $\varphi(\tau - \xi^*) = 1$ (point 'c'), $\varphi(\tau) = 0$ (point 'd'), $\varphi(\tau + \xi^*) = -1$ (point 'e'), $\varphi(2\tau - \xi^*) = -1$ (point 'f'), and $\varphi(2\tau) = 0$ (point 'a').

Therefore the nonlinearity becomes

$$f(\varphi) := -V'(\varphi) = \begin{cases} \varphi, & 0 < \xi < \xi^* \\ -\varphi + 2, & \xi^* < \xi < \tau - \xi^* \\ \varphi, & \tau - \xi^* < \xi < \tau + \xi^* \\ -\varphi - 2, & \tau + \xi^* < \xi < 2\tau - \xi^* \\ \varphi, & 2\tau - \xi^* < \xi < 2\tau. \end{cases} \tag{23}$$

On the intervals $(0, \xi^*)$, $(\tau - \xi^*, \tau + \xi^*)$, and $(2\tau - \xi^*, 2\tau)$, the differential equation is

$$(c^2 - 1)\varphi''(\xi) = \varphi(\xi)$$

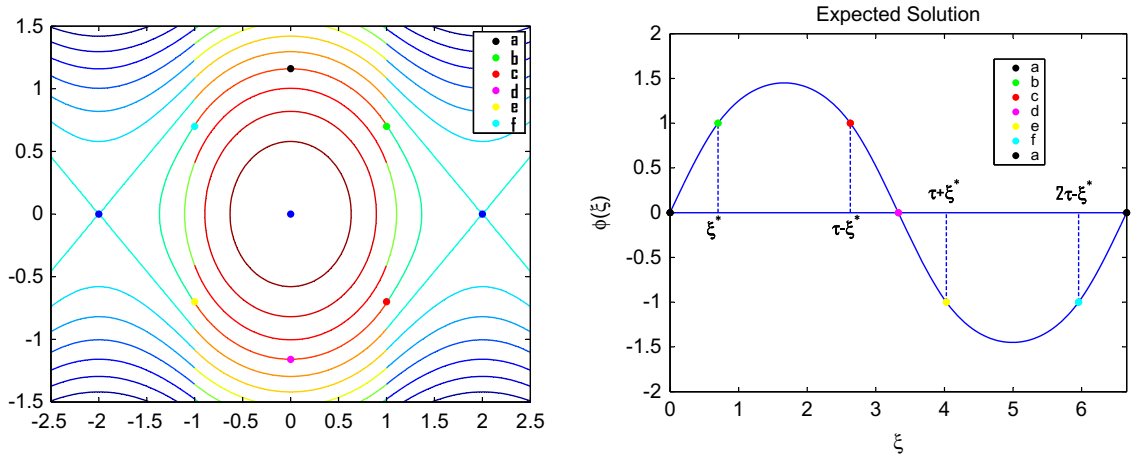


**Figure 11.** Phase portrait (left) and expected solution (right) of the nonlinear wave equation with sawtooth nonlinearity.

with general solution

$$\varphi(\xi) = c_1 \cos\left(\frac{\xi}{\sqrt{1-c^2}}\right) + c_2 \sin\left(\frac{\xi}{\sqrt{1-c^2}}\right)$$

where $c_1, c_2$ are different constants for each interval determined by the interval's boundary conditions

$$\begin{gathered} 0 < \xi < \xi^*, \varphi(0) = 0, \varphi(\xi^*) = 1, \\ \tau - \xi^* < \xi < \tau + \xi^*, \varphi(\tau - \xi^*) = 1, \varphi(\tau + \xi^*) = -1, \\ 2\tau - \xi^* < \xi < 2\tau, \varphi(2\tau - \xi^*) = -1, \varphi(2\tau) = 0. \end{gathered}$$

On $(\xi^*, \tau - \xi^*)$ we have

$$(c^2 - 1)\varphi''(\xi) = -\varphi(\xi) + 2$$

with general solution

$$\varphi(\xi) = c_3 e^{\frac{\xi}{\sqrt{1-c^2}}} + c_4 e^{\frac{-\xi}{\sqrt{1-c^2}}} + 2$$

where $c_3, c_4$ are constants determined by the boundary conditions $\varphi(\xi^*) = \varphi(\tau - \xi^*) = 1$. On $(\tau + \xi^*, 2\tau - \xi^*)$ we have the general solution

$$\varphi(\xi) = c_5 e^{\frac{\xi}{\sqrt{1-c^2}}} + c_6 e^{\frac{-\xi}{\sqrt{1-c^2}}} - 2$$

where $c_5, c_6$ are constants determined by the boundary conditions $\varphi(\tau + \xi^*) = \varphi(2\tau - \xi^*) = -1$. Figure 12 show solutions to the nonlinear wave equation with sawtooth nonlinearity for different values of $\xi^*$ and fixed $c$.

### 2.2.2. Discrete travelling waves

We now examine the periodic solutions of the discrete travelling wave equation (7) with sawtooth nonlinearity (22). As in the continuous case, for solutions of the form shown in Figure 11, equation becomes linear in $\varphi$ where $-V'(\varphi)$ is given in (23).

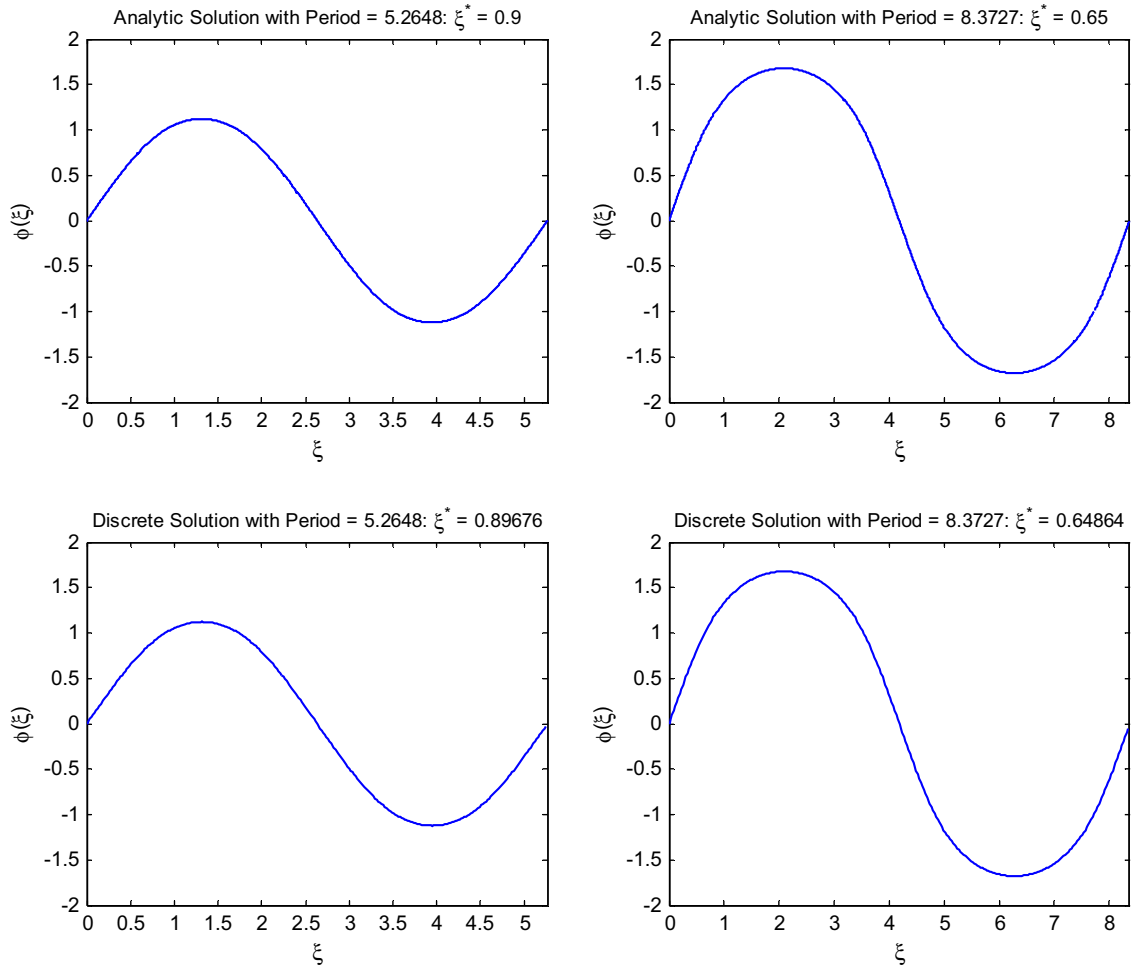


**Figure 12.** Comparison of the analytic solution and the discrete solution of the nonlinear wave equation with sawtooth nonlinearity, for fixed periods and fixed $c$, for irrational values of $\frac{\sigma}{\kappa}$.

Following Section 2.1.3, we expand both sides of (7) in a Fourier series, obtaining

$$\tilde{\varphi}_n d_n = \tilde{f}_n. \tag{24}$$

where $d_n$ is given in (21). Since $f(\varphi(\xi))$ is a periodic function with fixed period, $2\tau$, for fixed $c$ and each of the five intervals in the nonlinearity (23), the Fourier coefficients $\tilde{f}_n$ can be found explicitly and are given by

$$\begin{aligned}
\tilde{f}_n &= \frac{1}{2\tau}\int_0^{2\tau} f(\varphi(\xi))e^{-in\frac{\pi}{\tau}\xi}\,\mathrm{d}\xi \\
&= \frac{1}{2\tau}\left[\int_0^{\xi^*} \varphi(\xi)e^{-in\frac{\pi}{\tau}\xi}\,\mathrm{d}\xi + \int_{\xi^*}^{\tau-\xi^*} (-\varphi(\xi)+2)e^{-in\frac{\pi}{\tau}\xi}\,\mathrm{d}\xi\right. \\
&\quad \left. + \int_{\tau-\xi^*}^{\tau+\xi^*} \varphi(\xi)e^{-in\frac{\pi}{\tau}\xi}\,\mathrm{d}\xi + \int_{\tau+\xi^*}^{2\tau-\xi^*} (-\varphi(\xi)-2)e^{-in\frac{\pi}{\tau}\xi}\,\mathrm{d}\xi + \int_{2\tau-\xi^*}^{2\tau} (\varphi(\xi))e^{-in\frac{\pi}{\tau}\xi}\,\mathrm{d}\xi\right] \\
&= \sum_{k=-\infty}^{\infty} A_{kn}\tilde{\varphi}_n + b_n
\end{aligned}$$

where

$$A_{kn} = \frac{1+(-1)^{(k-n)}}{i(k-n)\pi}\left(e^{i(k-n)\frac{\pi}{\tau}\xi^*} - e^{-i(k-n)\frac{\pi}{\tau}\xi^*}\right)$$
$$b_n = \frac{1-(-1)^n}{in\pi}\left(e^{-in\frac{\pi}{\tau}\xi^*} + e^{in\frac{\pi}{\tau}\xi^*}\right).$$

Substituting this into (24) and solving for $\tilde{\varphi}_n$ we get,

$$\tilde{\varphi}_n = (\mathrm{diag}(d) - A)^{-1} b. \tag{25}$$

Thus far it appears that finding a travelling wave only requires solving a linear system. However, there is one final condition that needs to be imposed, and this one is nonlinear. This is the compatibility condition $\varphi(\xi^*) = 1$, which has to be solved numerically. The piecewise-linear force has reduced the problem to solving a scalar nonlinear equation in one variable. Our algorithm for finding discrete travelling waves is thus: (i) Fix the parameters $c$, $\sigma$, $\kappa$, and $\tau$. (ii) Choose a suitable initial number $N$ of Fourier modes with which to represent $\varphi$, and an initial guess for $\xi^*$ equal to that corresponding to the analytic solution with the same value of $\tau$. (iii) Solve equation $\varphi(\xi^*) = 1$ numerically. This involves repeatedly forming and solving an $N \times N$ linear system. (iv) Increase $N$ and examine the convergence of the Fourier series. In practice, we found that the nonlinear solve was extremely easy. The main drawback of the algorithm is that the linear solves limit the value of $N$ that can be used.

Discrete numerical solutions are plotted and compared with the analytic solution in Figure 12. It appears that the discrete numerical solutions are very similar to the analytic solution. This was confirmed by plotting the discrete solutions on top of the analytic solutions for fixed periods, varying the ratio $\sigma/\kappa$. In all cases tried, for both rational and irrational $\sigma/\kappa$, the discrete numerical solution seemed to match the corresponding analytic solution closely. No wiggles or lack of convergence were observed. Thus, the piecewise linear model appears to be a promising candidate for further study.

### 2.3. Smooth V′: Sine nonlinearity

Our final choice of nonlinearity is a smooth nonlinear function. We choose the sine function, so that our nonlinear wave equation becomes the sine-Gordon equation

$$u_{tt} = u_{xx} - \sin u. \tag{26}$$

Thus, we take $V'(\varphi) = \sin(\varphi)$ in equations (3) and (7). Again, there are periodic and heteroclinic travelling waves.

We use a pseudospectral Newton continuation method to find periodic travelling waves. We will be working in both real space and Fourier space so make the following definitions. Let $-\sin(\varphi(\xi)) = f(\varphi(\xi))$. Discrete periodic travelling waves will be approximated by the Fourier series

$$\varphi(\xi) = \sum_{n=-N}^{N} \tilde{\varphi}_n e^{in\frac{\pi}{\tau}\xi}$$

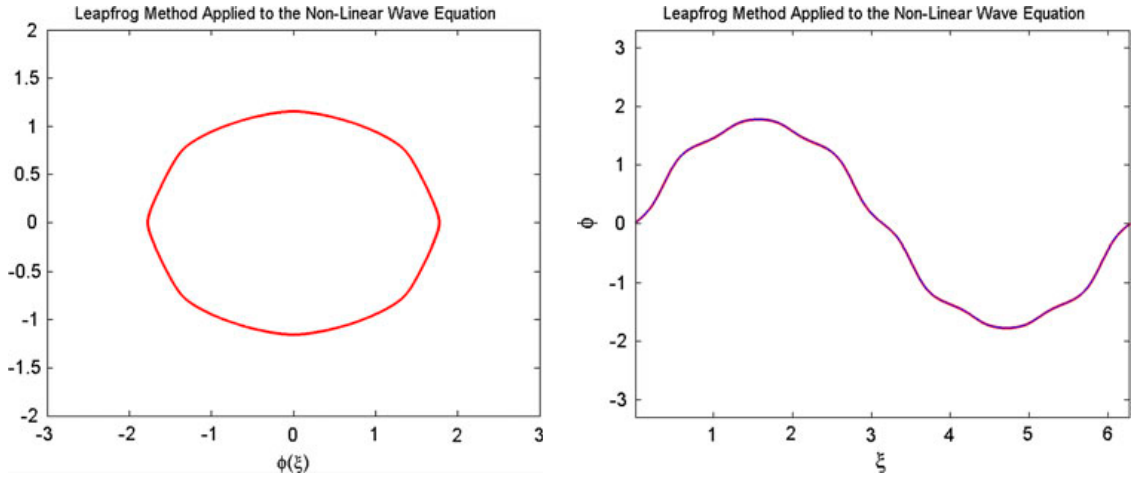


(a) Orbit of leapfrog applied to (3)

(b) Red: Solution of leapfrog applied to (3). Blue: Numerical solution of (7)

**Figure 13.** A comparison of solutions of (3) and (7) for $\sigma = \kappa = 0.8$.

where $T = 2\tau$ is the period of the solution. As in Section 2.2.2 we have

$$D\tilde{\varphi} = \tilde{f} \tag{27}$$

where $D = \text{diag}(d)$, with $d$ defined in (21). In real space,

$$L\varphi = f(\varphi) \tag{28}$$

where $L = \mathcal{F}^{-1}D\mathcal{F}$ is a linear operator, $\varphi = (\varphi(in\pi\xi/\tau))_{i=0}^{N}$, $\mathcal{F}\varphi = \tilde{\varphi}$, and $\mathcal{F}$ is the discrete Fourier transform.

We solve the nonlinear Equation (28) using Newton's method,

$$\varphi^{j+1} = \varphi^j - (L - \text{diag}(f'(\varphi^j))^{-1}(L\varphi^j - f(\varphi^j)).$$

Generally we hold $\sigma, \kappa$, and $c$ fixed and apply continuation in the parameter $T$ starting from its minimum value $T = 2\pi$. If we have quadratic convergence of Newton's method, and the Fourier coefficients $\tilde{\varphi}_n$ are decreasing rapidly, indicating convergence of the Fourier series, then this numerical solution will be close to an exact solution of the discrete travelling wave Equation (7). This is what we observe in almost all cases, the exceptions to be noted later.

We first present a second, independent check that this numerical method yields correct solutions to the discrete travelling wave Equation (7). When $\sigma = \kappa$ the discrete travelling wave Equation (7) is equivalent to finding periodic solutions of the leapfrog method applied to the pendulum problem, which is relatively well understood. We compare the orbit of the leapfrog method applied to (3) with initial conditions taken from a solution of the pseudospectral – Newton method. An example is shown in Figure 13 for $\sigma = \kappa = 0.8$ (known to be resonant), and the two solutions agree.

Figure 14 shows a sequence of solutions from the continuation. There are two distinct types of solution, those that are smooth we call non-resonant, those that possess noticeable

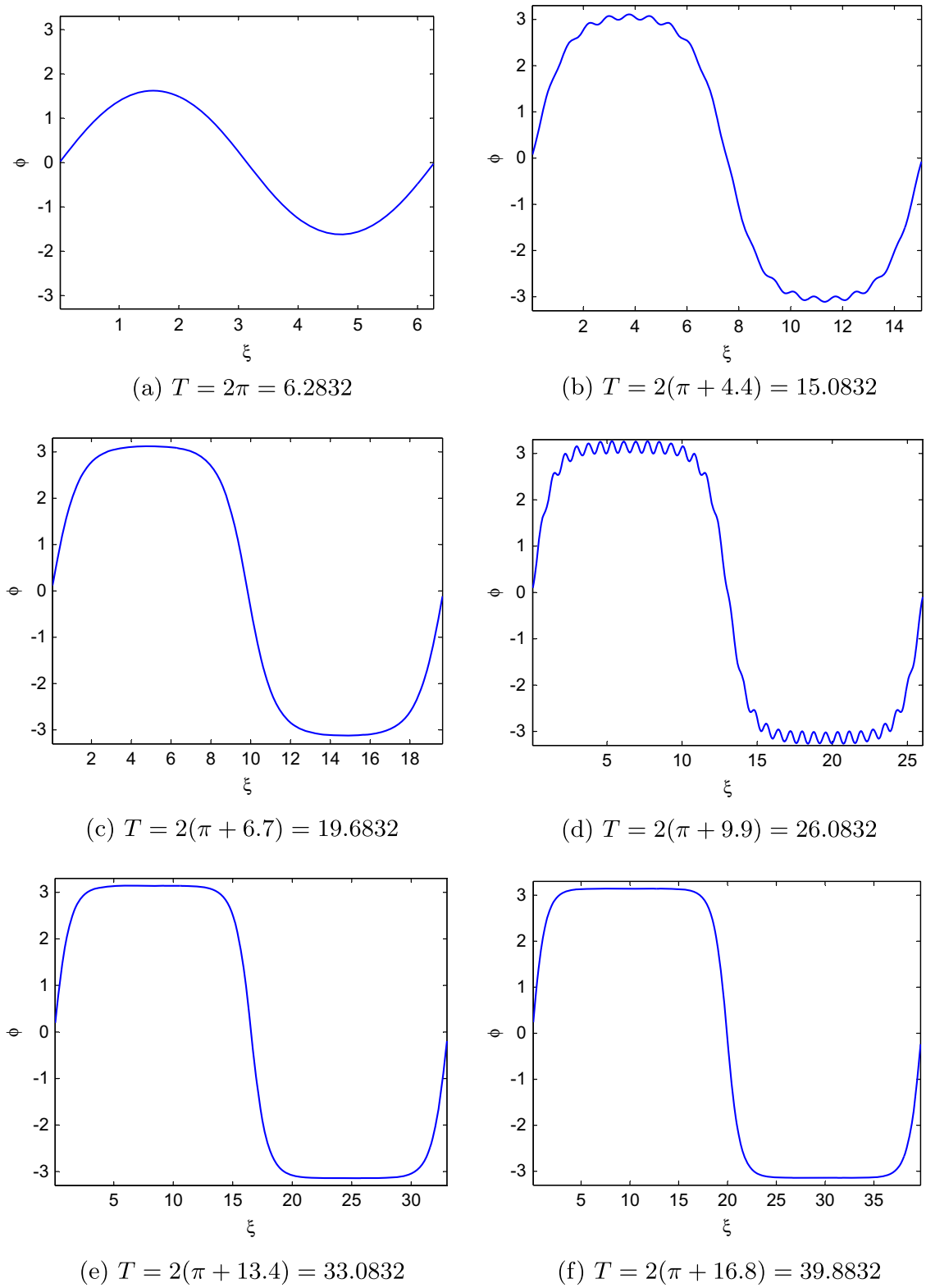


(a) $T = 2\pi = 6.2832$

(b) $T = 2(\pi + 4.4) = 15.0832$

(c) $T = 2(\pi + 6.7) = 19.6832$

(d) $T = 2(\pi + 9.9) = 26.0832$

(e) $T = 2(\pi + 13.4) = 33.0832$

(f) $T = 2(\pi + 16.8) = 39.8832$

**Figure 14.** Continuation in $T$ starting with $T = 2\pi$ for $\sigma = 1, \kappa = \frac{1}{\sqrt{2}}, c = 1.3$.

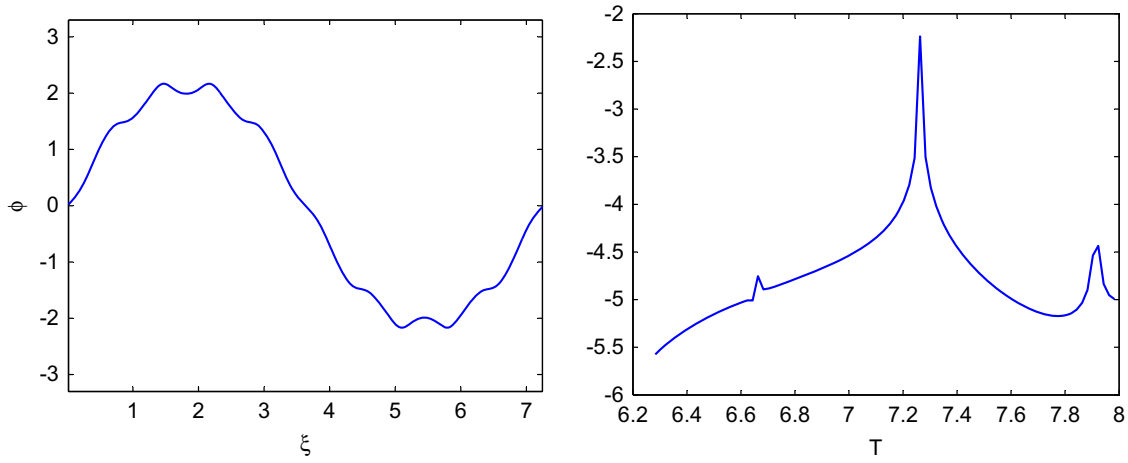


(a) $T = 2(\pi + 0.49) = 7.2632$ (b) Resonances

**Figure 15.** A short continuation in $T$ showing one major resonance peak. The $y$-axis gives the size of the resonance defined by (29).

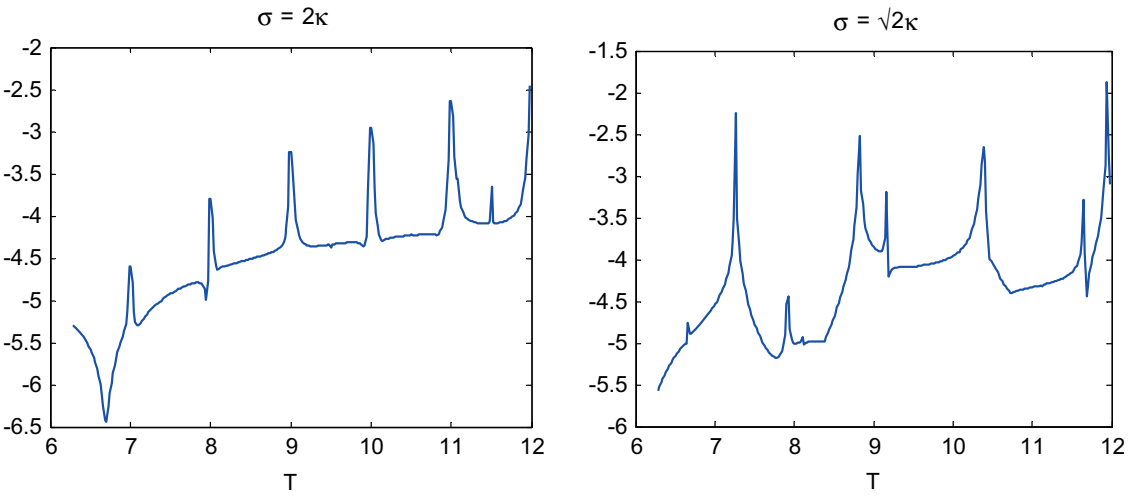


**Figure 16.** Comparison of the resonances for a rational ratio of $\frac{\sigma}{\kappa}$ and an irrational one. The $y$-axis gives the size of the resonance defined by (29).

wiggles are resonant. As the period increases so does the amplitude of the wave solution. As the period tends to infinity the solution tends to a heteroclinic travelling wave.

To quantify the resonances we use an ad-hoc measure based on the observation that smooth solutions for large $T$ are very flat near $\xi = T/4$. After some experimentation the function

$$R := \log_{10}\left(\max_{0.2T<\xi<0.3T} |d''| - \min_{0.2T<\xi<0.3T} |d''|\right). \tag{29}$$

was found to be a useful measure of resonance amplitude and was able to detect resonances. The resonance amplitude $R$ against the period of the solution is shown in Figure 15(b), in which the major peak showing corresponds to the solution shown in Figure 15(a).

Next, we plot the resonance for a slightly longer continuation simulation in Figure 16 and compare it for a rational ratio of $\frac{\sigma}{\kappa}$ and an irrational one. From this first investigation

it seems that the resonances for a rational ratio of $\frac{\sigma}{\kappa}$ are evenly spaced for increasing value of $T$, but for the irrational ratio, the resonances appear to occur more randomly.

When $\frac{\sigma}{\kappa} = m_1/m_2$, $\sigma$ and $\kappa$ are both integer multiples of $\kappa/m_2$. We would thus expect to see resonances when $T/(\kappa/m_2)$ is rational, and strong resonances when it is an integer, which has been confirmed experimentally [21]. However, it appears that not *every* integer value of $T/(\kappa/m_2)$ produces an equally strong resonance.

## 3. Part II. backward error analysis

To better understand how well multisymplectic discretisations preserve travelling wave solutions for nonlinear equations, we turn to backward error analysis. Indeed, similar studies have been performed in the past. Specifically, implicit midpoint time discretisations of the KdV equation [11] and the nonlinear Schrödinger equation [12] initialized with an exact travelling wave have better properties of error propagation than other (non-conservative) methods. From another point of view, initializing (5) with the heteroclinic travelling wave solution of the modified equation for the scheme produces a numerical solution that is accurate to higher order [28]. In the following subsection we consider modified equations for the same discretisation (5) and show that they have Hamiltonian structure with periodic travelling wave solutions that match the computed travelling wave to higher order. Then, we show how this idea can be extended to other multi-symplectic discretisations and other multi-Hamiltonian PDEs.

### 3.1. Smooth but arbitrary V′

We regard the coincidence between (7) and a symmetric linear multistep method, that holds when $\sigma/\kappa$ is rational, merely as an *analogy*. Since backward error analysis explains a good part of long-time behaviour of symmetric linear multistep methods (in particular, of their underlying one-step method), we apply backward error analysis directly to (7) for arbitrary $\sigma/\kappa$. We first write the second order ODE (3) as

$$\ddot{y} = f(y), \qquad f(y) = \frac{-V'(y)}{c^2 - 1}, \tag{30}$$

and the discrete travelling wave Equation (7) as

$$\frac{\frac{c^2}{\kappa^2}\big(y(t+\kappa) - 2y(t) + y(t-\kappa)\big) - \frac{1}{\sigma^2}\big(y(t+\sigma) - 2y(t) + y(t-\sigma)\big)}{c^2 - 1} = f(y(t)). \tag{31}$$

Using Taylor series expansions, we get

$$y(t \pm \kappa) = e^{\pm \kappa D} y(t) \qquad \text{and} \qquad y(t \pm \sigma) = e^{\pm \sigma D} y(t),$$

where $D$ is the total derivative with respect to $t$. Substituting these into (31) we get

$$L_{\kappa,\sigma} y(t) := \frac{\frac{c^2}{\kappa^2}\big(e^{\kappa D} - 2 + e^{-\kappa D}\big) - \frac{1}{\sigma^2}\big(e^{\sigma D} - 2 + e^{-\sigma D}\big)}{c^2 - 1} y(t) = f(y(t)) \tag{32}$$

where we define the linear operator $L_{\kappa,\sigma}$. Thus, there exist functions $f_i(\varphi, \dot{\varphi})$, polynomial in $(\sigma, \kappa)$ of degree $i-1$, such that every solution of the modified differential equation

$$\ddot{y} = f(y) + f_3(y, \dot{y}) + f_5(y, \dot{y}) + \cdots \tag{33}$$

satisfies (7) up to any order in $(\sigma, \kappa)$, where $f(y)$ is given in (30).

To illustrate, we carry out the required calculations up to the fourth order term by expanding the linear operator $L_{\kappa,\sigma}$ in a Taylor series up to terms of degree 4 in $(\sigma, \kappa)$. Rearranging (32) and applying the derivative $D$ twice gives

$$\ddot{y} = D^2 L_{\kappa,\sigma}^{-1} f(y) = (1 + \mu_2(\kappa, \sigma)D^2 + \mu_4(\kappa, \sigma)D^4 + \dots)f(y). \tag{34}$$

where

$$\mu_2 = \frac{\sigma^2 - c^2\kappa^2}{12(c^2-1)}, \qquad \mu_4 = \frac{3c^2\kappa^4 + 3\sigma^4 + 2c^2(\kappa^4 - 5\kappa^2\sigma^2 + \sigma^4)}{720(c^2-1)^2}.$$

Now, the derivatives $D^2 f(y)$ and $D^4 f(y)$ need to be calculated, giving expressions involving $f(y)$ and its derivatives and also derivatives of $y$, i.e. (33) for $\ddot{y}$, giving

$$D^2 f(y) = f''(y)\dot{y}^2 + f'(y)\ddot{y} = f''(y)\dot{y}^2 + f'(y)f(y) + \mathcal{O}(\sigma^2, \kappa^2).$$

Substituting this back into (34) and matching the coefficients of terms quadratic in $(\sigma, \kappa)$ with (33), we get

$$f_3(y, \dot{y}) = \mu_2(f''(y)\dot{y}^2 + f'(y)f(y)) \tag{35}$$

At the next (quartic) order we find $D^4 f(y)$ and comparing the coefficients of terms of degree 4 in $(\sigma, \kappa)$ we get

$$\begin{aligned} f_5(y, \dot{y}) =& \mu_2(f'(y)f_3(y, \dot{y})) + \mu_4(f'(y)^2 f(y) + 3f''(y)f(y)^2 + 5f''(y)\dot{y}^2 f'(y) \\ &+ 6f^{(3)}(y)\dot{y}^2 f(y) + f^{(4)}(y)\dot{y}^4). \end{aligned}$$

Each $f_n$ can be found similarly.

Now, it can be checked through direct calculation, that the modified differential Equation (33) for the discrete travelling wave equation can be written up to any power of $\sigma$ and $\kappa$ as a first-order planar noncanonical Hamiltonian system

$$\dot{z} = \widetilde{J}^{-1}(z)\nabla\widetilde{H}(z), \tag{36}$$

where $z \in \mathbb{R}^2$, $\widetilde{J} \in \mathbb{R}^{2\times 2}$ is a symplectic structure matrix, and $\widetilde{H}(z)$ is the modified Hamiltonian with expansion

$$\widetilde{H}(y, \dot{y}) = H(y, \dot{y}) + H_3(y, \dot{y}) + H_5(y, \dot{y}) + \cdots. \tag{37}$$

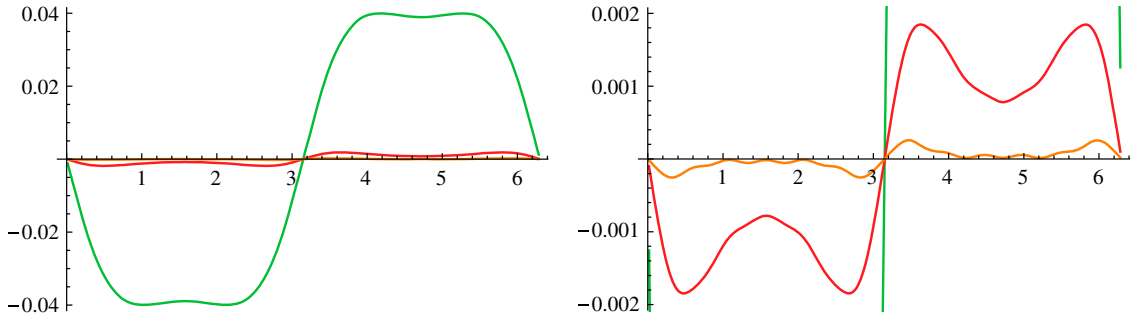


**Figure 17.** The errors $y - y_1$ (green), $y - y_2$ (red), and $y - y_3$ (orange) for a non-resonant periodic travelling wave of the form depicted in Figure 14 (zoomed on right).

Here each term $H_i$ is of degree $i - 1$ in $(\sigma, \kappa)$. We compute the first few terms in the modified Hamiltonian to be

$$H_3 = \frac{1}{2}\mu_2 f(y)^2 - \mu_2 f'(y)p^2$$
$$H_5 = \mu_4 f(y)^2 f'(y) + \frac{1}{2}(\mu_2^2 - 3\mu_4) f'(y)^2 p^2 - 2\mu_4 f(y) f''(y)\dot{y}^2 - \mu_4 p^4 f^{(3)}(y),$$

where $z = (y, p)$, and the modified symplectic structure is

$$J^{-1} = \begin{bmatrix} 0 & \widetilde{K} \\ -\widetilde{K} & 0 \end{bmatrix}, \tag{38}$$

where $\widetilde{K} = 1 + K_3 + K_5 + \cdots$, and

$$K_3 = 2\mu_2 f'(y), \qquad K_5 = -(\mu_2^2 - 3\mu_4) f'(y)^2 + 4\mu_4 f(y) f''(y) - 4\mu_4 p^2 f'''(y).$$

Thus the travelling waves of the modified equation can be read off from the level sets of $\widetilde{H}$. As this is a smooth function close to $H$, we see that, in the sense of backward error analysis, all periodic and all heteroclinic travelling waves are preserved by the integrator.

We can get some idea of the validity of the method by comparing a computed travelling wave $y$ with the solutions of the modified differential equation determined by backward error analysis. Figure 17 gives these solutions for $T = 2\pi, \sigma = \kappa = 0.5$, where

$$y_1 \text{ is the solution of } \ddot{y} = f(y)$$
$$y_2 \text{ is the solution of } \ddot{y} = f(y) + \mu_2 f_3(y, \dot{y})$$
$$y_3 \text{ is the solution of } \ddot{y} = f(y) + \mu_2 f_3(y, \dot{y}) + \mu_4 f_5(y, \dot{y}),$$

which are computed numerically using NDSolve in Mathematica, with $f(y) = \sin(y)/(1 - c^2)$. Although the space and time steps are fairly large, the modified equation gives an excellent approximation to the actual travelling waves, with more terms improving the accuracy.

We next compare, in Figure 18, the resonance measure $R$ given in Equation (29) of the actual travelling waves and those of the modified equation. We see that the modified equation does not capture the resonant behaviour. (The same phenomenon is seen for

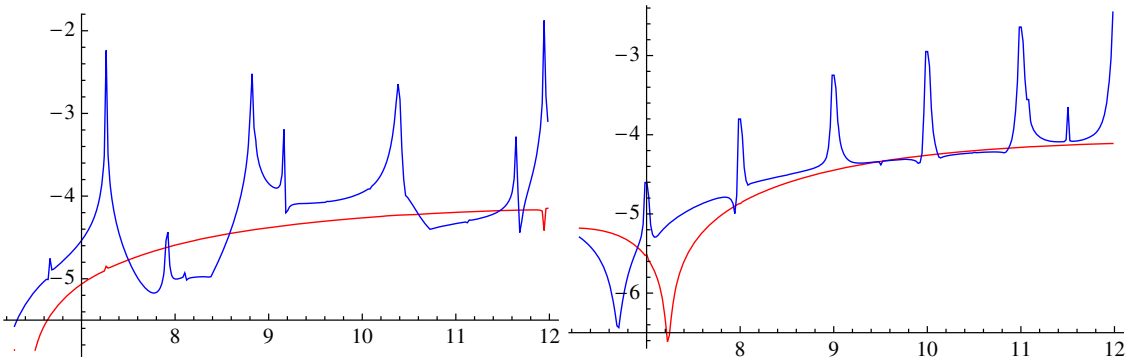


**Figure 18.** Resonance measure $R$ of the numerical solution from Section 2.3 given by the blue curve. Resonance measure $R$ of the modified differential equation for the discrete travelling wave equation given by the red curve.

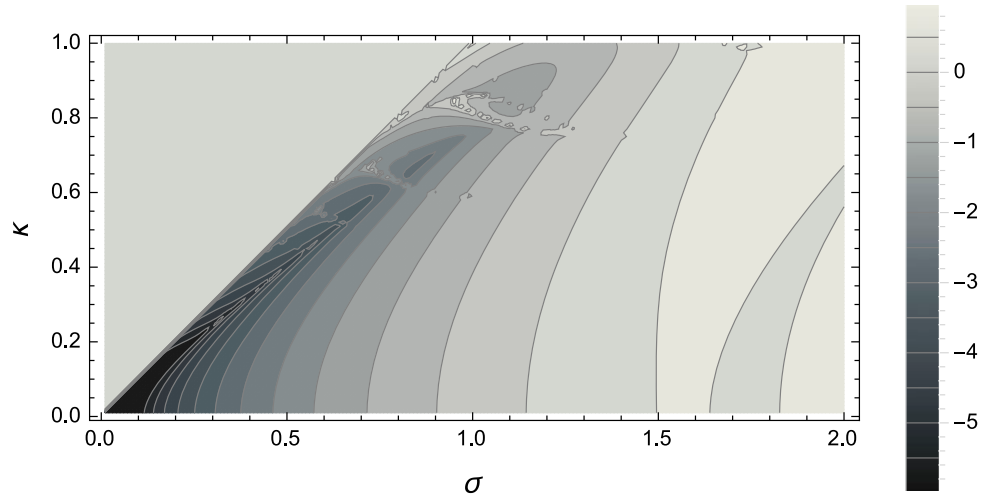


**Figure 19.** Contour plot of $\log_{10} \|y - y_2\|_2$ for $\kappa \leq \sigma$ where $y$ is a discrete travelling wave and $y_2$ is the corresponding solution of the first truncation of the modified equation. Here $T = 2\pi$ and $c = 1.3$.

ODEs.) However, it does approximate the actual travelling waves very accurately in this sensitive measure.

Finally, for fixed values of $T$ and $c$, we compare the actual travelling waves and those predicted from the modified equation for all $\sigma$ and $\kappa$. Figure 19 shows a contour plot of $\log_{10} \|y - y_2\|_2$ where $y$ is a discrete travelling wave and $y_2$ is the corresponding solution of the first truncation of the modified equation. Overall, the error behaviour is that predicted by the Taylor series (the smooth part of figure), and the resonances show up as small anomalies. Only two such anomalies (near $(\sigma, \kappa) = (0.8, 0.6)$ and $(1.0, 0.8)$) are at all significant.

### 3.2. Generalizations to other methods and PDEs

The same method of backward error analysis can be used to approximate the travelling wave solutions of any multisymplectic integrator for any multiHamiltonian problem. We illustrate this using the Preissman box scheme, a multisymplectic integrator that can (unlike the leapfrog method considered earlier) be applied to any multi-Hamiltonian PDE. This

gives

$$(KD_tM_x + LD_xM_t)z_i^n = \nabla S(M_tM_xz_i^n), \tag{39}$$

where $D_tz_i^n = (z_i^{n+1} - z_i^n)/(\Delta t)$, $D_xz_i^n = (z_{i+1}^n - z_i^n)/(\Delta x)$, $M_xz_i^n = (z_i^n + z_{i+1}^n)/2$, and $M_t = (z_i^n + z_i^{n+1})/2$.

Substituting travelling wave coordinates we get the difference operators

$$D_\xi^\kappa\varphi(\xi) = -\frac{c(\varphi(\xi) - \varphi(\xi-\kappa))}{\kappa}, \qquad D_\xi^\sigma\varphi(\xi) = \frac{\varphi(\xi+\sigma) - \varphi(\xi)}{\sigma},$$
$$M_\xi^\kappa\varphi(\xi) = \frac{(\varphi(\xi) + \varphi(\xi-\kappa))}{2}, \qquad M_\xi^\sigma\varphi(\xi) = \frac{\varphi(\xi) + \varphi(\xi+\sigma)}{\sigma},$$

so that upon substituting travelling wave coordinates in the discretisation (39) we get the system of difference equations,

$$(KD_\xi^\kappa M_\xi^\sigma + LD_\xi^\sigma M_\xi^\kappa)\varphi(\xi) = \nabla S(M_\xi^\kappa M_\xi^\sigma\varphi(\xi)). \tag{40}$$

If the linear operator on the left is nonsingular, we can move it to the right hand side and apply the $\xi$ derivative $D$ to both sides to get

$$\dot\varphi(\xi) = D((KD_\xi^\kappa M_\xi^\sigma + LD_\xi^\sigma M_\xi^\kappa)^{-1}\nabla S(M_\xi^\kappa M_\xi^\sigma\varphi(\xi)). \tag{41}$$

As before, the right hand side can be expanded in a Taylor series in $(\sigma,\kappa)$ which allows the modified equation to be determined term-by-term. We expect that it will be conjugate to symplectic and thus the preservation of travelling waves, in the sense of backward error analysis, can be determined from the Hamiltonian of the continuous travelling wave equation.

This occurs, for example, in the nonlinear Schrödinger equation

$$i\psi_t + \psi_{xx} + 2|\psi|^2\psi = 0, \qquad \psi \in \mathbb{C}.$$

Setting $\psi = p + iq$, $\psi_x = v + iw$, the multi-Hamiltonian form is (1) with

$$z = \begin{bmatrix} p \\ q \\ v \\ w \end{bmatrix}, \qquad K = \begin{bmatrix} 0 & -1 & 0 & 0 \\ 1 & 0 & 0 & 0 \\ 0 & 0 & 0 & 0 \\ 0 & 0 & 0 & 0 \end{bmatrix}, \qquad L = \begin{bmatrix} 0 & 0 & 1 & 0 \\ 0 & 0 & 0 & 1 \\ -1 & 0 & 0 & 0 \\ 0 & -1 & 0 & 0 \end{bmatrix}$$

and $S = -\frac{1}{2}(p^2+q^2) - \frac{1}{2}(v^2+w^2)$. Equation (41) in this case becomes

$$\dot\varphi(\xi) = D\begin{bmatrix} 0 & 0 & -\frac{1}{D_\xi^\sigma M_\xi^\kappa} & 0 \\ & 0 & 0 & -\frac{1}{D_\xi^\sigma M_\xi^\kappa} \\ \frac{1}{D_\xi^\sigma M_\xi^\kappa} & 0 & 0 & -\frac{D_\xi^\kappa M_\xi^\sigma}{(D_\xi^\kappa M_\xi^\sigma)^2} \\ 0 & \frac{1}{D_\xi^\sigma M_\xi^\kappa} & \frac{D_\xi^\kappa M_\xi^\sigma}{(D_\xi^\kappa M_\xi^\sigma)^2} & 0 \end{bmatrix}\nabla S(M_\xi^\kappa M_\xi^\sigma\varphi(\xi)).$$

The modified equation of the discrete travelling waves is a 4-dimensional noncanonical Hamiltonian system. Both the continuous and the modified systems are rotationally invariant. Thus, travelling waves are generically preserved in this example. For 4-dimensional systems without such a symmetry, more complicated situations can arise. For example, the continuous travelling wave equation may be integrable while the modified equation for discrete travelling waves is not integrable. In this case not all travelling waves would be preserved. However, even in this case the backward error analysis gives considerable insight in the preservation of dynamics.

The method can also be applied if the linear operator in (40) is singular. We illustrate this for the nonlinear wave Equation (1) in the formulation

$$z = \begin{bmatrix} u \\ v \\ w \end{bmatrix}, \qquad K = \begin{bmatrix} 0 & 1 & 0 \\ -1 & 0 & 0 \\ 0 & 0 & 0 \end{bmatrix}, \qquad L = \begin{bmatrix} 0 & 0 & -1 \\ 0 & 0 & 0 \\ 1 & 0 & 0 \end{bmatrix},$$

and $S(z) = -V(u) + \frac{1}{2}(w^2 - v^2)$.

The multi-Hamiltonian discretisation (39) for the leapfrog (i.e. the standard 5-point) discretisation of the nonlinear wave equation may be written

$$(KD_t + LD_x)z_i^n = \nabla S(z_i^n) \tag{42}$$

where

$$D_t z_i^n = \frac{z_i^{n+\frac{1}{2}} - z_i^{n-\frac{1}{2}}}{\Delta t}, \qquad D_x z_i^n = \frac{z_{i+\frac{1}{2}}^n - z_{i-\frac{1}{2}}^n}{\Delta x}. \tag{43}$$

In matrix form (42) becomes

$$\begin{bmatrix} 0 & D_t & -D_x \\ -D_t & 0 & 0 \\ D_x & 0 & 0 \end{bmatrix} z_i^n = \nabla S(z_i^n).$$

Letting

$$D_\xi^\gamma \varphi(\xi) = \frac{\varphi(\xi + \frac{1}{2}\gamma) - \varphi(\xi - \frac{1}{2}\gamma)}{\gamma}, \tag{44}$$

the discrete travelling wave equation is

$$(LD_\xi^\sigma - cKD_\xi^\kappa)\varphi(\xi) = \nabla S(\varphi(\xi)),$$

and in matrix form,

$$\begin{bmatrix} 0 & -cD_\xi^\kappa & -D_\xi^\sigma \\ cD_\xi^\kappa & 0 & 0 \\ D_\xi^\sigma & 0 & 0 \end{bmatrix} \varphi(\xi) = \nabla S(\varphi(\xi)), \tag{45}$$

The operator on the left hand side is singular. We eliminate $\varphi_3$ using the last equation, move the remaining linear operator to the right hand side, and apply $D$ to both sides to get

$$\dot{\varphi} = D \begin{bmatrix} 0 & (cD_\xi^\kappa)^{-1} \\ -cD_\xi^\kappa (c^2 (D_\xi^\kappa)^2 - (D_\xi^\sigma)^2)^{-1} & 0 \end{bmatrix} \begin{bmatrix} -V'(\varphi_1) \\ -\varphi_2 \end{bmatrix}.$$

The right hand side can be expanded in a Taylor series to produce the modified equation, which is used to study the phase portraits of the modified Hamiltonian. This approach provides an alternative route to the modified equation derived previously in Equations (36) and (37).

It can be seen that the ideas and methods developed here apply to higher-dimensional wave equations and to the preservation of travelling waves of general multi-Hamiltonian systems by very large classes of multisymplectic integrators.

## 4. Discussion

The standard application of backward error analysis for symplectic integrators reduces an $N$-dimensional symplectic map to an $N$-dimensional Hamiltonian flow. This is essentially a reduction by one dimension. The present application of backward error analysis, in conjunction with the travelling wave reduction, has reduced an infinite-dimensional map to a two-dimensional Hamiltonian ODE, a far more spectacular reduction. This is even more striking in view of the fact that there is no accepted backward error analysis for partial difference equations in general (see [27]).

Thus, we see that backward error analysis is exceptionally powerful for this problem, reducing the intractable functional Equation (7) to a simple planar Hamiltonian ODE. Furthermore, by comparing the phase portraits of the original and modified systems we see that any orbits that are structurally stable, that is any orbits that are also present up to small perturbations in nearby Hamiltonian systems, are preserved. This includes periodic and heteroclinic travelling waves for the sine-Gordon equation, although this result is not specific to the sine-Gordon equation or its integrability and holds (generically) for any potential. This preservation holds in the sense of backward error analysis, that is, up to any power of the time and space step sizes.

This situation in the ODE case, analyzing the preservation of phase portraits by symplectic integrators, can be studied using the language of topological equivalence. It is shown in [23] that for generic smooth Hamiltonians $H$, the level sets of $H$ and of the modified Hamiltonian $\widetilde{H}$ of a symplectic integrator are topologically equivalent. It is in this sense that, in the two-dimensional case, symplectic integrators preserve all orbits. Thus, we can expect, for example, that if a travelling wave corresponds to a topologically unstable orbit of the travelling wave equation, then it will not be preserved by typical multisymplectic integrators. This, however, is an exceptional case, and even in higher dimensions we can expect that typical travelling waves, whose existence is due to preserved features of the travelling wave equation like dimension and linear symmetries, will be preserved by multisymplectic integrators.

Although the numerical examples given above suggest that the modified vector field is a very good approximation to the travelling waves, which in direct numerical calculations do appear to exist, of course this is no substitute for a rigorous proof of their existence. Instead, we regard the backward error analysis as suggesting the mechanism by which travelling waves can be preserved and as a guide to the development of good numerical methods.

## Disclosure statement

No potential conflict of interest was reported by the authors.

## Funding

G.R.W. Quispel was supported by the Australian Research Council.

## References

[1] U.M. Ascher, and R.I. McLachlan, *Multisymplectic box schemes and the Korteweg–de Vries equation*, Appl. Numer. Math. 48 (2004), pp. 255–269.
[2] T.J. Bridges, *Multi-symplectic structures and wave propagation*, Math. Proc. Cambridge 121 (1997), pp. 147–190.
[3] T.J. Bridges, *A geometric formulation of the conservation of wave action and its implications for signature and the classification of instabilities*, Proc. R. Soc. Lond. A 453 (1997), pp. 1365–1395.
[4] T.J. Bridges, and G. Derks, *Unstable eigenvalues and the linearization about solitary waves and fronts with symmetry*, Proc. R. Soc. Lond. A 455 (1999), pp. 2427–2469.
[5] T.J. Bridges, and G. Derks, *The symplectic Evans matrix, and the instability of solitary waves and fronts*, Arch. Ration. Mech. An. 156 (2001), pp. 1–87.
[6] T.J. Bridges, and S. Reich, *Multi-symplectic integrators: Numerical schemes for Hamiltonian PDEs that conserve symplecticity*, J. Phys. A: Math. Gen. 284 (2001), pp. 184–193.
[7] T.J. Bridges, and S. Reich, *Numerical methods for Hamiltonian PDEs*, J. Phys. A 39 (2006), pp. 5287–5320.
[8] J.W. Cahn, J. Mallet-Paret, and E.S. Van Vleck, *Traveling wave solutions for systems of ODE's on a two-dimensional spatial lattice*, SIAM J. Appl. Math. 59 (1998), pp. 455–493.
[9] G. Cohen, *Higher-order numerical methods for transient wave equations*, Springer, Berlin, 2002.
[10] C.J. Cotter, D.D. Holm, and P.E. Hydon, *Multisymplectic formulation of fluid dynamics using the inverse map*, Proc. R. Soc. Lond. A 463 (2007), pp. 2671–2687.
[11] J. De Frutos, and J.M. Sanz-Serna, *Accuracy and conservation properties in numerical integration: the case of the Korteweg-de Vries equation*, Numer. Math. 75 (1997), pp. 421–445.
[12] A. Duran, and J.M. Sanz-Serna, *The numerical integration of relative equilibrium solutions: The nonlinear Schrödinger equation*, IMA J. Numer. Anal. 20 (2000), pp. 235–261.
[13] J. Frank, *Conservation of wave action under multisymplectic discretization*, J. Phys. A: Math. Gen. 39 (2006), pp. 5479–5493.
[14] J. Frank, B.E. Moore, and S. Reich, *Linear PDEs and numerical methods that preserve a multi-symplectic conservation law*, SIAM J. Sci. Comput. 28(1) (2006), pp. 260–277.
[15] E. Hairer, C. Lubich, and G. Wanner, *Geometric Numerical Integration: Structure-Preserving Algorithms for Ordinary Differential Equations*, Springer Series in Computational Mathematics Vol. 31, Springer, Berlin, 2002.
[16] J.L. Hong, Y. Liu, and G. Sun, *The multi-symplecticity of partitioned Runge–Kutta methods for Hamiltonian PDEs*, Math. Comput. 75 (2005), pp. 167–181.
[17] A.L. Islas, and C.M. Schober, *On the preservation of phase space structure under multisymplectic discretization*, J. Comput. Phys. 197 (2004), pp. 585–609.
[18] B. Leimkuhler, and S. Reich, *Simulating Hamiltonian Dynamics*, Cambridge University Press, Cambridge, 2004.
[19] H. Liu, and K. Zhang, *Multi-symplectic Runge-Kutta-type methods for Hamiltonian wave equations*, IMA J. Numer. Anal. 26(2) (2006), pp. 252–271.
[20] J.E. Marsden, G.W. Patrick, and S. Shkoller, *Multisymplectic geometry, variational integrators, and nonlinear PDEs*, Commun. Math. Phys. 199(2) (1998), pp. 351–395.
[21] F.C. McDonald, *Travelling wave solutions of multisymplectic discretisations of wave equations*, Ph.D. thesis, Massey University, 2013.
[22] M.P. McKean, *Nagumo's equation*, Adv. Math. 4 (1970), pp. 209–223.
[23] R.I. McLachlan, M. Perlmutter, and G.R.W. Quispel, *On the nonlinear stability of symplectic integrators*, BIT 44 (2004), pp. 99–117.

[24] R.I. McLachlan, and G.R.W. Quispel, *Geometric integrators for ODEs*, J. Phys. A 39(19) (2006), pp. 5251–5286.
[25] R.I. McLachlan, B.N. Ryland, and Y. Sun, *High order multisymplectic Runge–Kutta methods*, SIAM J. Sci. Comput. 36 (2014), pp. A2199–A2226.
[26] R.I. McLachlan, Y. Sun, and P.S.P. Tse, *Linear stability of partitioned Runge–Kutta methods*, SIAM J. Numer. Anal. 49(1) (2011), pp. 232–263.
[27] B.E. Moore, and S. Reich, *Backward error analysis for multi-symplectic integration methods*, Numer. Math. 95(4) (2003), pp. 625–652.
[28] B.E. Moore, and S. Reich, *Multi-symplectic integration methods for Hamiltonian PDEs*, Future Gener. Comput. Sy. 19(21) (2003), pp. 395–402.
[29] S. Reich, *Multi-symplectic Runge–Kutta collocation methods for Hamiltonian wave equations*, J. Comput. Phys. 157 (2000), pp. 473–499.
[30] B.N. Ryland, *Multisymplectic integration*, Ph.D. thesis, Massey University, 2007.
[31] B.N. Ryland, and R.I. McLachlan, *On multisymplecticity of partitioned Runge–Kutta methods*, SIAM J. Sci. Comput. 84(6) (2007), pp. 847–869.

## Appendix 1. Steady state solutions

To understand how multi-symplectic methods compare to other popular methods, consider the steady-state solutions of (5). These represent the limiting case of travelling waves of zero speed. The discrete travelling wave equation reduces to the leapfrog method applied to the continuous travelling wave equation. Thus, its behaviour is well known and we summarize it here from two points of view.

First, for small $\Delta x$, backward error analysis shows how solutions to (5) satisfy extremely closely (up to terms exponentially small in $\Delta x$) a 'modified equation' which is also a planar Hamiltonian system. Thus, in this sense of backward error analysis, comparing the steady-state solutions of (5) and (2) amounts to comparing the phase portraits of two planar Hamiltonian systems with nearby Hamiltonians. Generic periodic orbits and hetero/homoclinic orbits persist, and, for the leapfrog method, which we are considering here, some nongeneric ones persist, too. This point of view is developed further in [23].

Second, for finite $\Delta x$, the phase portrait of the leapfrog method for generic potentials is, to some extent, well understood. Where the continuous problem has a hetero/homoclinic orbit, the discrete problem will have two orbits. Likewise, periodic orbits of the discrete problem come in pairs that approximate continuous periodic orbits of the continuous problem. These provide periodic solutions of the discrete problem on infinite and on periodic domains. According to KAM theory, strongly nonresonant periodic solutions of the continuous problem persist and thus provide periodic discrete solutions on an infinite domain.

In contrast, non-symplectic spatial discretizations, such as upwind differences, show a completely different behaviour. Their steady state equation corresponds to the application of a non-symplectic integrator, such as Euler's method, to the reduced travelling wave equation. Typically, all hetero/homoclinic orbits, and but a finite number of periodic orbits (typically one), are destroyed by such a discretization.

We can also use the steady-state case to compare multisymplectic schemes with *symmetric* ones. The relationship between symplectic and symmetric methods is now well understood in numerical ODEs, but is not always appreciated in numerical PDEs. For example, Cohen [9, p.34] writes "All the schemes described below will be centred, since uncentred schemes generate numerical dissipation for wave equations which satisfy a principle of energy conservation." In fact, for the problem considered here, symmetric methods only preserve symmetric waves. Consider the force $-V'(u) = f(u) = \sin u + \frac{2}{5}\cos 2u$. The ODE $u_{xx} = -f(u)$, which here describes steady states of (2), was used in [15] to study non-conservation of energy by symmetric integrators. This ODE is time-reversible, but has non-symmetric orbits. In contrast, in the ODE $u_{xx} = -\sin(u)$ (describing steady states of the sine – Gordon equation), almost all orbits are symmetric with respect to the reversing symmetry $u \to -u$, $x \to -x$. It is necessary to break this symmetry to see the influence of non-symmetric orbits.

Equation (4) with $c = 0$ has the phase portrait given in Figure A1. From this we see that the PDE has both periodic and heteroclinic steady states, but no homoclinic steady states. We choose one of

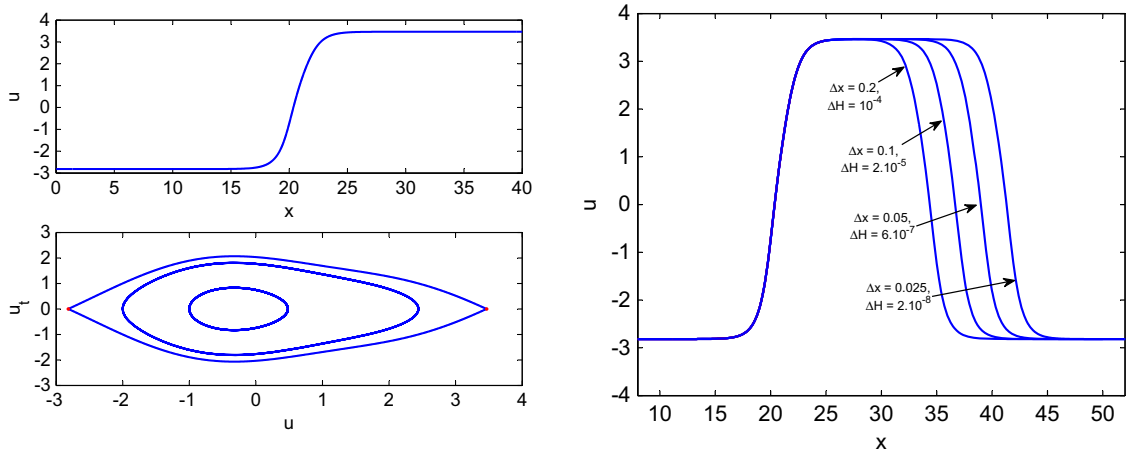


**Figure A1.** Left: Exact solutions of steady-state solutions of (2) with $-V'(u) = \sin u + \frac{2}{5}\cos 2u$ (top: one of two heteroclinic solutions; bottom: phase portrait showing two heteroclinic and two periodic orbits.) Right: Steady state solutions of a symmetric spatial discretisation (Lobatto IIIA); there are homoclinic, but no heteroclinic orbits for any $\Delta x$.

the heteroclinic orbits and plot the corresponding solution on the left-hand side of Figure A1. The ODE (4) does have a reversing symmetry, namely $(\varphi, \psi, x) \to (\varphi, -\psi, -t)$, but the heteroclinic orbits are not symmetric under this reversing symmetry.

The 3-stage Lobatto IIIA method is applied in space to (2) with $-V'(u) = \sin u + \frac{2}{5}\cos 2u$. This Runge–Kutta method is symmetric but not symplectic. The steady state solutions of the method are the same as the solutions of the same RK method applied to (4). We calculate the solutions that are asymptotic to the fixed point near $(\varphi, \psi) = (-\pi, 0)$, and find that the method has no heteroclinic steady states for any of the values of $\Delta x$ considered, but it does have homoclinic steady states. These are shown on the right-hand side of Figure A1 and indicate that the method has no heteroclinic steady states for any $\Delta x$, but it does have homoclinic steady states. These are formed by gluing together a heteroclinic wave and its reflection a distance $\log(\Delta x)$ apart. That is, the symmetric method has a qualitatively wrong steady state structure for all $\Delta x$.

The above treatment of discrete steady-state solutions also gives a description of some discrete travelling wave solutions, those with speed $c = \Delta x/\Delta t$. Their profile moves one grid point to the right per time step, i.e. $u_i^n = \varphi(x_i - \frac{\Delta x}{\Delta t} t_n)$. They obey the discrete travelling wave equation

$$\left(\frac{1}{(\Delta t)^2} - \frac{1}{(\Delta x)^2}\right)\big(\varphi((i+1)\Delta x) - 2\varphi(i\Delta x) + \varphi((i-1)\Delta x)\big) + V'(\varphi(i\Delta x)) = 0$$

which, for $\Delta x \neq \Delta t$, is equivalent to the steady-state case of (7). Thus, the preservation of these travelling waves by the 5-point scheme is identical to its preservation of steady states. In the limiting case of $c = 1$ and $\Delta t = \Delta x$, the waves obey equation $V'(\varphi(i\Delta x)) = 0$, which (but for the discreteness) is identical to the continuous version $V'(\varphi(\xi)) = 0$.